Results in Chemistry 4 (2022) 100629

Contents lists available at ScienceDirect

Results in Chemistry

journal homepage: www.sciencedirect.com/journal/results-in-chemistry

Adsorption of methylene blue on magnetite humic acid: Kinetic, isotherm, thermodynamic, and regeneration studies

Nur Ahmad [a,c], Fitri Suryani Arsyad [b], Idha Royani [b], Aldes Lesbani [b,c,*]

[a] Magister Program in Environment Management, Sriwijaya University, Jl. Padang Salasa No. 524 Ilir Barat 1, Palembang, 30139, South Sumatera, Indonesia
[b] Graduate School, Faculty of Mathematics and Natural Sciences, Sriwijaya University, Jl. Palembang-Prabumulih, Km.90-32, Ogan Ilir, South Sumatera, Indonesia
[c] Research Center of Inorganic Center of Inorganic Materials and Complexes, Faculty of Mathematics and Natural Sciences, Sriwijaya University, Jl. Padang Salasa No. 524 Ilir Barat 1, Palembang, 30139, South Sumatera, Indonesia

ARTICLE INFO

Keywords:
Adsorption
Magnetite humic acid
Methylene blue

ABSTRACT

Preparation of Magnetite Humic Acid (MHA) 3:1, 2.5:1, 2:1, and 1.5:1 was successful as evidenced by the characterization using FTIR, XRD, VSM, SEM-EDS analysis. The FTIR spectra have a typical absorption at 3425, 1604, 1396, 1095, 1026, 910, 794, and 540 cm^{-1}. XRD patterns show diffraction peaks at $2\theta = 20.40$ °, 35.63°, and 63.3°. MHA 3:1, 2.5:1, 2:1, and 1.5:1 was paramagnetic with magnetization (Ms) at 20.44, 17.04, 15.51, and 13.82 emu/g, respectively. The surface of MHA is smooth because it is prepared by hydrothermal process. Fe atom appear after HA is composited into MHA. The percent mass of Fe atom in MHA were 3:1, 2.5:1, 2:1, 1.5:1, at 34.5 %, 31.5 %, 27.7 %, and 24.4 %, respectively. The percent mass of Fe atom decreases in line with the VSM analysis which decreases the magnetization. The functional groups of HA and MHA are total acidity, carboxyl group, and phenolic hydroxyl group. The carboxyl and phenolic hydroxyl groups are iodized and interact with Fe^{2+} and Fe^{3+} from Fe_3O_4. However, the carboxyl group is more interactive with Fe_3O_4 than the phenolic hydroxyl group, so the carboxyl group's reduction is very drastic. pHpzc of HA and MHA 3:1, 2.5:1, 2:1, 1.5:1 at 8.06, 5.82, 6.08, 4.80, and 4.76, respectively. HA and MHA were better at PSO and Langmuir model in adsorption of MB. Maximum adsorption capacity of HA and MHA 3:1, 2.5:1, 2:1, 1.5:1 at 66.225, 102.041, 161.290, 156.250, 138.889 mg/g, respectively. The highest maximum adsorption capacity is MHA 2.5:1 (161.290 mg/g). MHA 2.5:1 will be continued with regeneration. MHA regeneration efficiency decreased from 92.28 % to 58.92 % in the fifth cycle. These results indicate the good recyclability of MHA to remove MB supported by FTIR and XRD analysis after adsorption which shows no significant changes.

Introduction

In decade, synthetic dyes are increases use in the paper, textile, wood, hair, and cotton industries, one of which is methylene blue (MB) [1–3]. However, MB produces wastewater containing organic compounds that harm humans and aquatic life [4]. Therefore, this problem must be solved, which can reduce or even eliminate MB in waters [5–6]. Various methods have been used for removal of methylene blue, including photocatalytic [7], electrocoagulation [8], biodegradation [9], electrochemical [10], and adsorption [11]. Adsorption was chosen because the method is simple, low cost, and many available precursors with high adsorption capacity. In adsorption required an effective adsorbent for removal MB. Adsorbents of MB have been reported use activated bentonite, lignite waste, tea biochar, CuAl-LDH, apple pomace, orange peels, and humic acid [2,12–16].

Humic acid is a large organic polymer with a random structure with total acidity, carboxylic, and phenolic functional groups [17–18]. Humic acid is widespread, not only in soil but also found in water [19–20]. In addition, humic acid has been reported as an ion exchange, antibody responses, reduced capacity, and adsorbent [21–22]. Humic acid has been used as an adsorbent of heavy metals (Pb (II) and Cd (II)), ammonia, organic nitrogen, crystal violet dye, and malachite green dye [23–27]. Humic acid has a large surface area with high surface activity, so it can be used as an adsorbent [28]. However, humic acid does not have stability to recycle of the adsorbent because its structure collapses. To solve this problem thus humic acid should be composited with various materials, including lignite, bentonite, cellulose, and magnetite [25,29–30].

* Corresponding author.
E-mail address: aldeslesbani@pps.unsri.ac.id (A. Lesbani).

https://doi.org/10.1016/j.rechem.2022.100629
Received 12 October 2022; Accepted 4 November 2022
Available online 7 November 2022
2211-7156/© 2022 The Author(s). Published by Elsevier B.V. This is an open access article under the CC BY license (http://creativecommons.org/licenses/by/4.0/).

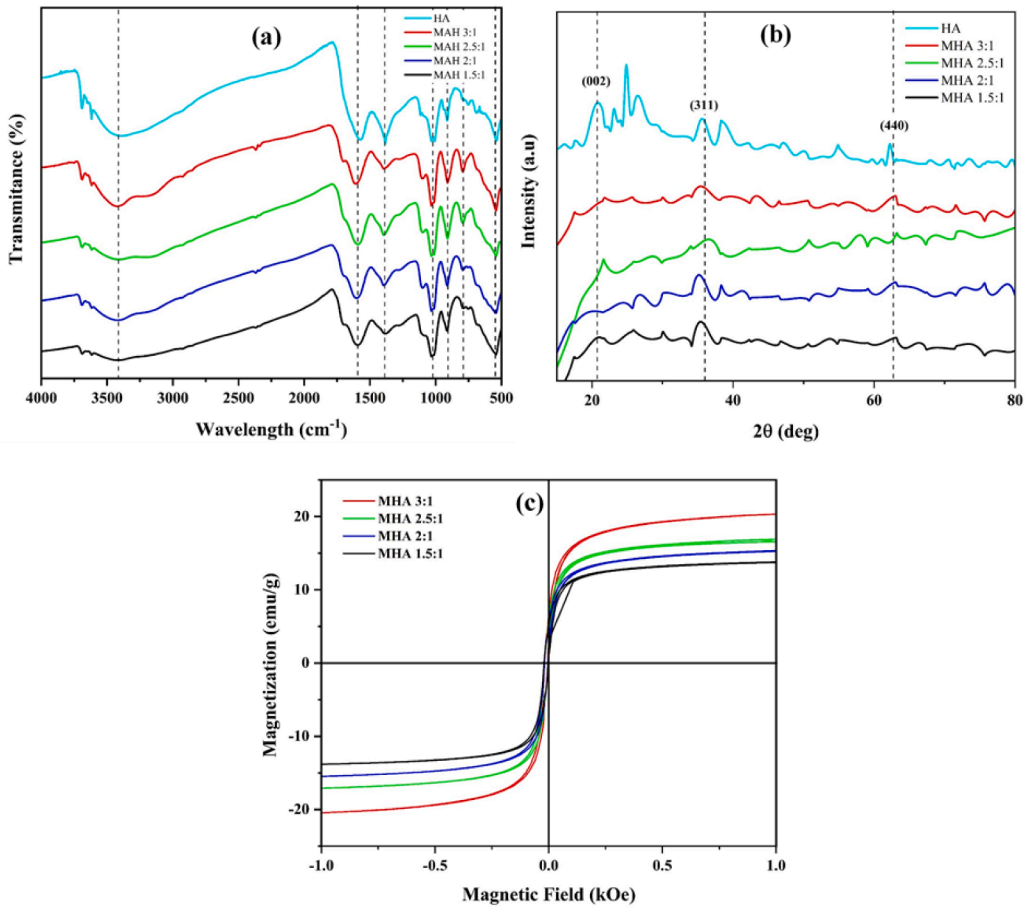

Fig. 1. Characterization of MHA: (a) FTIR spectra, (b) XRD patterns, and (c) VSM curve.

Magnetite is a mineral rock composed of iron oxide with the chemical formula Fe_3O_4 [31–33]. Magnetite is a very attractive mineral because of its Physico-chemical properties that can be used for various applications, i.e., water purification or thermal energy storage [34]. In recent decades, magnetite has been of great interest in the development of adsorbent materials, because makes it easy to separate the adsorbent and adsorbate using an external magnet [35]. Magnetite and humic acid will interact because of the high adsorption capacity of magnetite, the electrostatic attraction, and the presence of a carboxyl group on the surface of the humic acid in combination with ferrous cations [36]. Therefore, magnetite and humic are suitable to be composited into magnetite humic acid (MHA) and used to adsorption of MB. Composite magnetite with humic acid has been reported for removing phosphate [37], removing Pb (II) [24], and styryl pyridinium dye [38].

In the experiment part, humic acid (HA) was obtained from local soil in South Sumatera, Indonesia. Magnetite humic acid (MHA) was prepared in a ratio of 3:1, 2.5:1, 2:1, and 1.5:1 for repeat use of adsorbent. Characterization of adsorbent was carried out using FTIR, XRD, VSM, and SEM-EDS analysis to indicate the success of material synthesis. The functional groups of HA and MHA, namely total acidity, carboxyl group, and phenolic hydroxyl group were observed. Adsorption performances of HA and MHA were also investigated by pHpzc, kinetics, isotherms, and thermodynamics. The adsorbent with the highest adsorption capacity was continued with the regeneration process for 5 times to see the structural stability of the MHA.

Experimental

Materials

Humic Acid (HA) was obtained from local soil in South Sumatera, Indonesia. The chemical used, ferric chloride ($FeCl_3$) and ferrous sulfate ($FeSO_4{\cdot}7H_2O$) were purchased from Merck, hydrogen chloride (HCl) was purchased from MallinckrodtAR®, sodium hydroxide (NaOH), barium hydroxide ($Ba(OH)_2$), magnesium acetate ($Mg(CH_3COO)_2$), and ammonia (NH_3) were purchased from EMSURE® ACS. Distilled water was purchased from PT. Dira Sonita.

Preparation of magnetite humic acid (MHA)

Magnetite was prepared follow procedure Ahmad et al. [39] from a mixture of $FeCl_3$ (0.018, 0.015, 0.012, 0.009 mol) and $FeSO_4{\cdot}7H_2O$ (0.006 mol) in 9 mL distilled water, respectively. Magnetite solution added 3 g of humic acid, then shaken for 4 h.NH_3 (3 mL) was added slowly, then shaken for 30 min at 75 °C. MHA followed the hydrothermal process for 4 h at 150 °C, filtered and dried. MHA was prepared in a ratio of 3:1, 2.5:1, 2:1, and 1.5:1. MHA continued with the hydrothermal process for 4 h at 150 °C, filtered with Whatman paper (2.5μ m), and dried. MHA is made in a ratio 3:1, 2.5:1, 2:1, and 1.5:1.

Characterization

UV–Visible Spectrophotometer type Biobase BK-UV 1800 PC was used to measure the concentration of MB. Fourier Transfer Infra-Red (FTIR) type Shimadzu Prestige-21 was used to analyze the functional group. X-ray Diffractometer (XRD) type Rigaku Miniflex-6000 was used

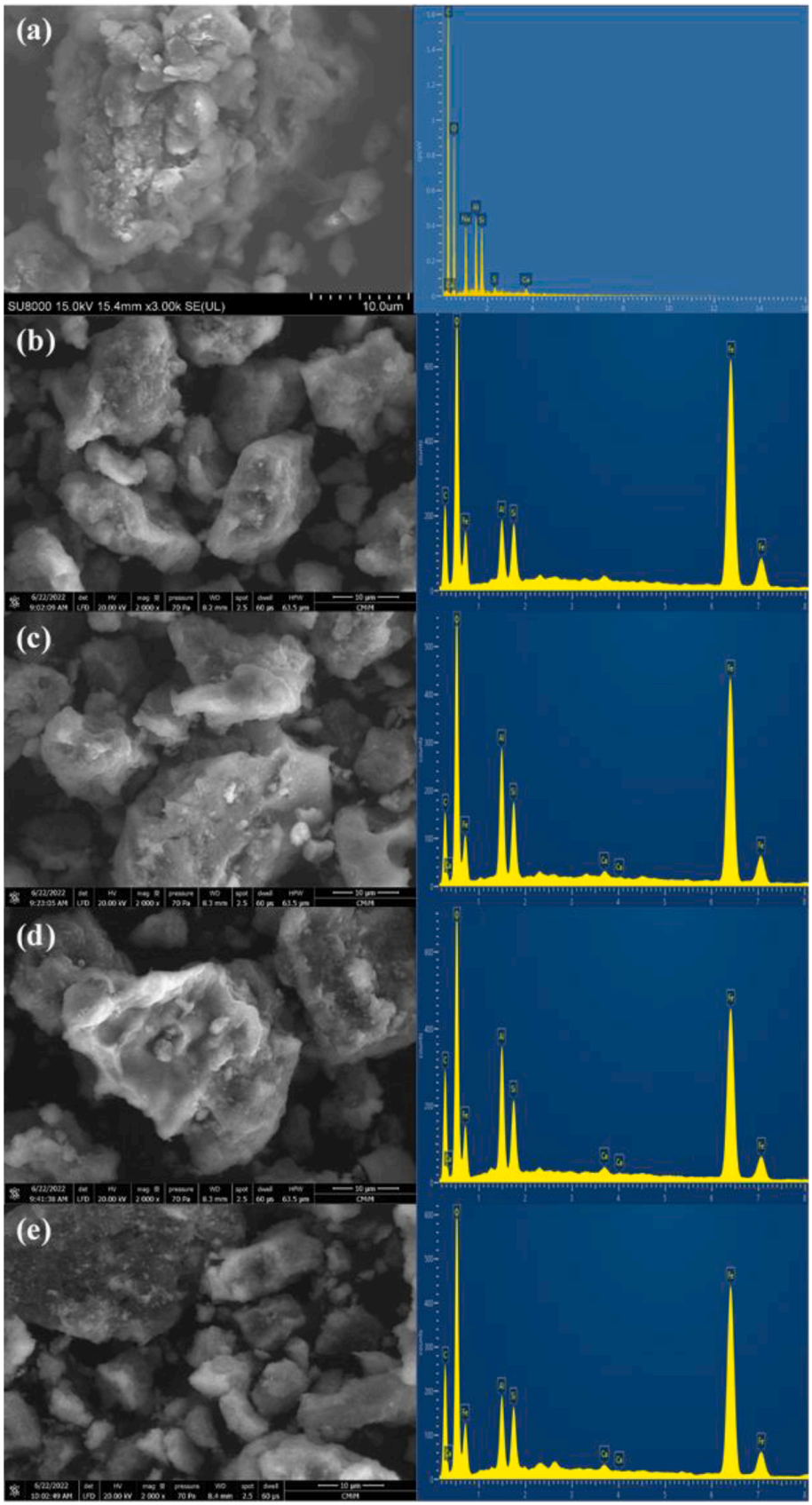

Fig. 2. SEM image (a) HA, (b) MHA 3:1, (c) MHA 2.5:1, (d) MHA 2:1, and (e) MHA 1.5:1.

Table 1
EDS of HA and MHA.

Element	HA (% wt)	MHA 3:1 (% wt)	MHA 2.5:1 (%wt)	MHA 2:1 (% wt)	MHA 1.5:1 (%wt)
Fe	–	34.5	31.5	27.7	24.4
C	55.7	29.8	28.6	34.7	35.4
O	14.8	31.1	31.5	32.6	32.9

Table 2
Total acidity, carboxyl group, and phenolic hydroxyl group of HA and MHA.

Adsorbent	Total acidity (cmol/kg)	Carboxyl group (cmol/kg)	Phenolic Hydroxyl group (cmol/kg)	Ref.
Humic acid	570–890	150–570	150–400	[50]
Humic acid	670	296	374	This study
MHA 3:1	287.50	37.33	250.17	This study
MHA 2.5:1	317.50	59.33	258.17	This study
MHA 2:1	405	42	363	This study
MHA 1.5:1	430	44.67	385.33	This study

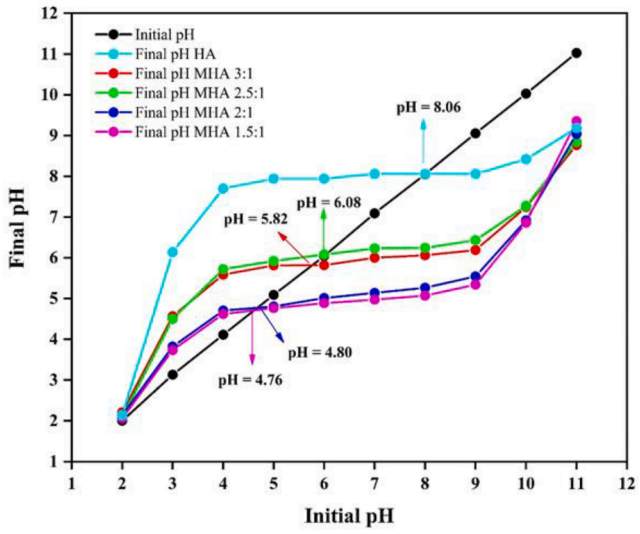

Fig. 3. pHpzc of HA and MHA.

to study the crystal morphology. Vibrating Sample Magnetometer (VSM) type OXFORD VSM1.2H was used to measure the magnetization of MHA. Scanning Electron Microscope Energy Dispersive Spectrometer (SEM-EDS) Quanta 650 OXFORD was used to analyze the surface morphology and element of HA and MHA.

Determination of functional group HA and MHA

Determination of functional group of HA and MHA was followed Santosa et al. [40]. The functional groups of HA and MHA, namely total acidity, carboxyl group, and phenolic hydroxyl group were observed.

Total acidity

100 mg of HA and MHA was added to 20 mL saturated solution Ba $(OH)_2$ under N_2 atmosphere and stirred for 24 h at 25 °C, filtered and washed. The filtrate and wash water were titrated with HCl (0.5 M) to pH 8.4. The total acidity MHA was determined using equation:

Table 3
Pseudo-first-order and pseudo-second-order kinetics parameters for the adsorption of MB by HA and MHA.

Kinetic Parameter	Parameter	Adsorbent HA	MHA 3:1	MHA 2.5:1	MHA 2:1	MHA 1.5:1
Pseudo First Order	Qe_{exp} (mg/g)	11.139	22.753	20.902	22.893	22.694
	Qe_{calc} (mg/g)	10.406	16.173	17.002	13.861	16.007
	k_1 (min^{-1})	0.020	0.033	0.030	0.036	0.020
	R^2	0.912	0.983	0.982	0.966	0.974
Pseudo Second Order	Qe_{exp} (mg/g)	11.139	22.753	20.902	22.893	22.694
	Qe_{calc} (mg/g)	12.788	24.213	22.779	23.981	24.631
	k_2 (g/mg. min)	0.002	0.004	0.003	0.005	0.002
	R^2	0.980	0.999	0.998	0.999	0.996

$$\text{Total acidity}\ (\text{cmol kg}^{-1}) = \frac{(V_0 - V_s) \times M \times 10^5}{W}$$

where V_0 and V_s are the volume of HCl for titrated blank solution and sample, respectively; M is the molarity of HCl; W is the mass of HA and MHA.

Carboxyl group

100 mg HA and MHA were added to 10 mL $Mg(CH_3COO)_2$ 0.5 M and 40 mL distilled water under N_2 atmosphere and stirred for 24 h at 25 °C, filtered and washed. The filtrate and wash water were titrated with NaOH (0.1 M) to pH 9.8. The carboxyl group MHA was determined using equation:

$$\text{Carboxyl group}\ (\text{cmol kg}^{-1}) = \frac{(V_0 - V_s) \times M \times 10^5}{W}$$

where V_0 and V_s are the volume of NaOH for titrated blank solution and sample, respectively; M is the molarity of NaOH; W is the mass of HA and MHA.

Phenolic hydroxyl group

The phenolic hydroxyl group was determined using equation:

$$\text{Phenolic hydroxyl group}\ (\text{cmol kg}^{-1}) = \text{Total acidity} - \text{Carboxyl group}$$

Adsorption experiments

Adsorption experiments were carried out in a 100 mL volumetric flask. Each flask was filled with 20 mL MB and 20 mg of HA and MHA 3:1, 2.5:1, 2:1, and 1.5:1, respectively. The mixture was shaken using a shaker (120 r/min). The effect of adsorption parameters on the adsorption process was investigated such as pHpzc with initial pH (2–11), contact time (0–180 min), temperature (303–343 K), and initial concentration (50–150 mg/L). pH value was adjusted with 0.1 M hydrogen chloride and 0.1 M sodium hydroxide. The MHA in the volumetric flask was separated from the MB solution using an external magnet. The filtrate was analyzed using UV–Vis$\lambda = 664$ nm. An adsorbent with the largest adsorption capacity will be followed by a regeneration process. The regeneration process was conducted by adding 20 mg adsorbents to 30 mg/L of MB 20 mL, shaken for 2 h. After that, the desorption of MB in 20 mL distilled water using an ultrasonic device for 15 min.

Models for kinetic studies

The adsorption kinetics were analyzed by pseudo-first-order (PFO) and pseudo-second-order (PSO) [39] with the following equation

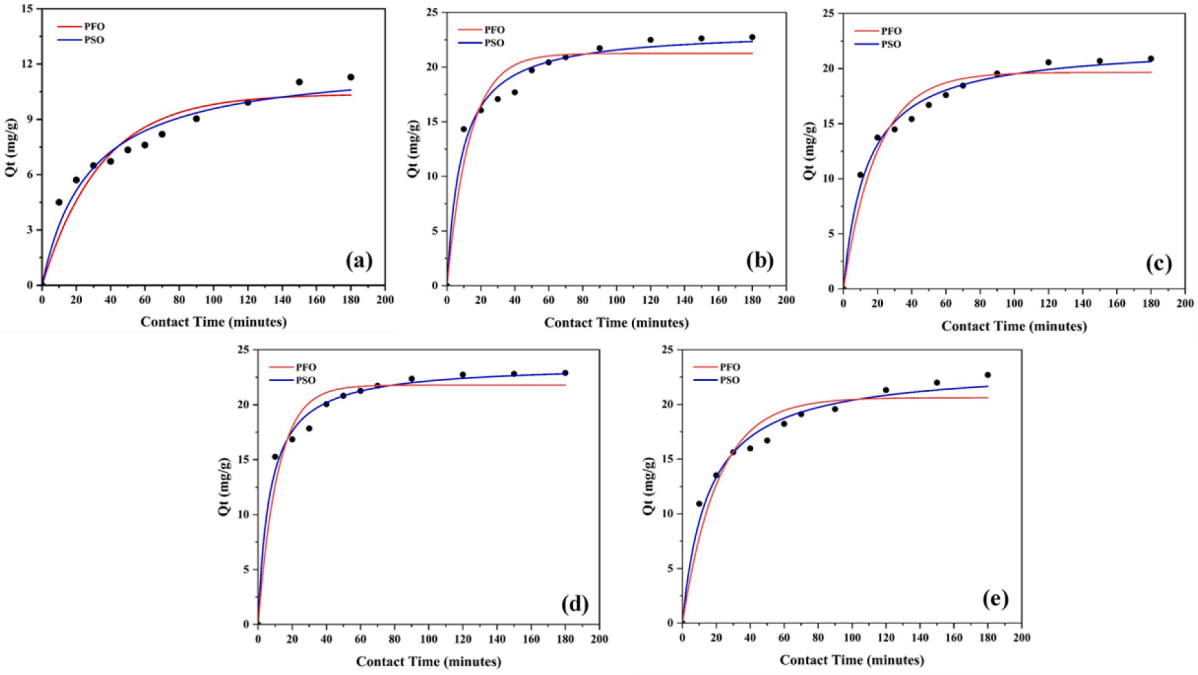

Fig. 4. Adsorption kinetics for MB 25 mg/L at (a) HA, (b) MHA 3:1, (c) MHA 2.5:1, (d) MHA 2:1, and (e) MHA 1.5:1.

Table 4
Langmuir and Freundlich ishotherms parameters for the adsorption of MB by HA and MHA.

Adsorbent	T (K)	Langmuir			Freundlich		
		Qmax	kL	R^2	n	kF	R^2
HA	303	66.225	0.034	0.9384	1.527	4.866	0.8431
	313	63.291	0.042	0.9224	1.697	6.665	0.8385
	323	62.893	0.046	0.9217	1.702	7.078	0.8433
	333	59.880	0.058	0.919	1.734	8.002	0.9004
	343	60.606	0.057	0.9187	1.622	7.306	0.8628
MHA 3:1	303	82.645	0.256	0.8083	6.464	41.333	0.4672
	313	88.496	0.251	0.8482	6.075	42.628	0.5139
	323	88.496	0.412	0.8181	6.258	45.740	0.7661
	333	93.458	0.360	0,8013	5.621	44.937	0.7123
	343	102.041	0.389	0.7987	5.056	47.011	0.6939
MHA 2.5:1	303	161.290	0.043	0.9952	1.831	31.915	0.8219
	313	147.059	0.067	0.9952	2.179	20.635	0.8199
	323	138.889	0.099	0.999	2.552	27.797	0.7108
	333	140.845	0.121	0.9987	2.675	32.063	0.5986
	343	140.845	0.156	0.998	3.058	39.683	0.4659
MHA 2:1	303	114.943	0.114	0.9778	2.946	27.290	0.8343
	313	126.582	0.152	0.9820	2.899	32.412	0.8285
	323	135.135	0.193	0.9833	2.640	35.530	0.8040
	333	144.928	0.252	0.9909	2.546	39.600	0.8645
	343	156.250	0.257	0.9791	2.353	41.238	0.8020
MHA 1.5:1	303	128.205	0.080	0.9739	2.538	22.851	0.9749
	313	113.636	0.368	0.9880	5.365	53.654	0.7520
	323	129.870	0.700	0.9972	4.013	60.506	0.7004
	333	138.889	0.393	0.9684	3.784	56.885	0.5117
	343	136.986	0.603	0.9930	3.388	58.385	0.6465

$$\log(Q_e - Q_t) = \log Q_e - \left(\frac{k_1}{2.303}\right) t (\boldsymbol{PFO})$$

$$\frac{1}{Q_t} = \frac{1}{k_2 {Q_e}^2} + \frac{1}{Q_e} (\boldsymbol{PSO})$$

where Q_e and Q_t are adsorption capacity at equilibrium and t, respectively (mg/g); k_1 (min^{-1}) and k_2 ($g/mg.min^{-1}$) are the rate constant at PFO and PSO, respectively; t is the adsorption time of MB.

Models for isotherm studies

The adsorption isotherms were analyzed by Langmuir and Freundlich isotherm model with the following equation

$$\frac{C_e}{Q_e} = \frac{C_e}{Q_m} + \frac{1}{Q_m K_L} (\boldsymbol{LangmuirIsotherm})$$

$$\log Q_e = \log K_F - 1/n \log C_e (\boldsymbol{FreundlichIsotherm})$$

where C_e (mg/L) and Q_e (mg/g) are the concentration of MB and adsorption capacity at equilibrium, respectively (mg/g); Q_m (mg/g) is

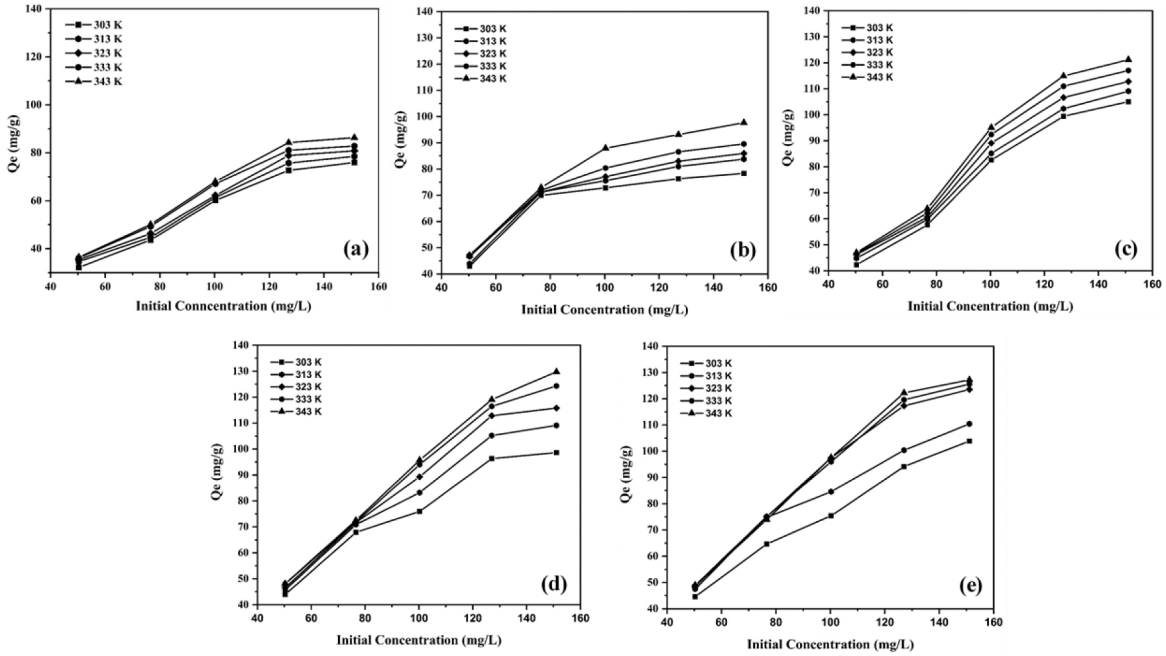

Fig. 5. Adsorption ishotherms on (a) HA, (b) MHA 3:1, (c) MHA 2.5:1, (d) MHA 2:1, and (e) MHA 1.5:1.

Table 5
The maximum adsorption capacity of different adsorbents for MB.

Adsorbent	Q*max* (mg/g)	Ref.
Chitosan Lignin Membrane	76.70	[1]
Apple Pomace	107.6	[2]
MIL101-Cr/PANI/Ag	43.29	[4]
Electrolytic Manganase Anone Slime (EMAS)	70.74	[56]
Hydrogels	26.04	[57]
Chitosan/K-carrageenan/acid-activated bentonite	18.80	[12]
Tea Biochar	105.27	[13]
ZrO_2@Rice Straw-Derived SiO_2	13.5	[58]
Calix[8]arene-Modified PbS	11.90	[59]
Geothermal silica	108	[60]
Lignite Waste	120	[16]
Orange Peels	142.86	[14]
CuAl-LDHs	58.803	[15]
HA	66.225	This study
MHA 3:1	102.041	This study
MHA 2.5:1	161.290	This study
MHA 2:1	156.250	This study
MHA 1.5:1	138.889	This study

the maximum adsorption capacity; K_L and K_F are the rate constant at Langmuir and Freundlich, respectively.

Adsorption thermodynamic

The thermodynamic equation and the Gibbs free energy were determined using equation:

$$\ln\frac{Q_e}{C_e} = \frac{\Delta S}{R} - \frac{\Delta H}{RT}\ (\boldsymbol{Thermodynamicequation})$$

$$\Delta G^{\circ} = \Delta H - T\Delta S(\boldsymbol{TheGibbsfreeenergy})$$

where C_e (mg/L) and Q_e (mg/g) are the concentration of MB and adsorption capacity at equilibrium, respectively (mg/g); ΔS (J/mol.K) is the entropy; ΔG° (kJ/mol) is the gibbs free energy. ΔH(kJ/mol) is the enthalpy; R (J/mol.K) is the gas constant; T (K) is the temperature.

Results and discussion

Characterization of MHA

FTIR analysis: As illustrated in Fig. 1a, the FTIR spectra of HA and MHA 3:1, 2.5:1, 2:1, 1.5:1, respectively. The peak at 3425 cm^{-1} is due to the phenolic hydroxyl group (OH) [41,42], 1604 cm^{-1} is related to C—C group stretching vibration of the aromatic ring [43], 1396 cm^{-1} as bending vibration of the carboxyl group ($HCOO^-$) [44], 1095 cm^{-1} as stretching vibration C—O—C, 1026, 910, and 540 cm^{-1} are stretching vibration from C—O [45]. The peaks at 794 cm^{-1} and indicate the presence of Fe-O [46–47].

XRD analysis: Fig. 1b shows the XRD patterns of HA and MHA 3:1, 2.5:1, 2:1, 1.5:1, respectively. HA and MHA show diffraction peaks at 2θ = 20.40 ° (0 0 2), 35.63° (3 1 1), and 63.3° (4 4 0). The diffraction peaks that appear are the characteristic peaks of magnetite [36,48]. The crystal structure of magnetite is affected after modification with humic acid. This is due to the electrostatic interaction of the negatively charged carboxylic group of humic acid to the positively charged functional

Table 6
Adsorption thermodynamics of MB by MHA.

Adsorbent	Δ H (kJ/mol)	Δ S (J/K.mol)	Δ G (kJ/mol) 303 K	313 K	323 K	333 K	343 K	R^2
HA	8.193	0.029	−0.722	−1.016	−1.311	−1.605	−1.899	0.996
MHA 3:1	12.059	0.043	−0.974	−1.404	−1.834	−2.264	−2.694	0.946
MHA 2.5:1	20.517	0.082	−4.453	−5.277	−6.101	−6.925	−7.749	0.998
MHA 2:1	25.297	0.089	−1.557	−2.443	−3.330	−4.216	−5.102	0.996
MHA 1.5:1	31.187	0.124	−6.472	−7.715	−8.958	−10.201	−11.443	0.952

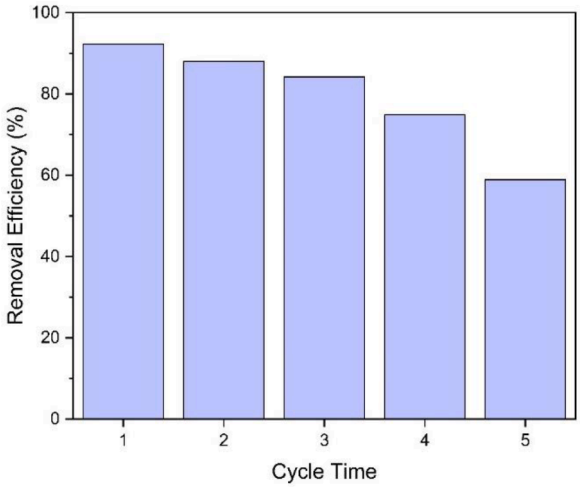

Fig. 6. Regeneration of MHA 2.5:1.

group of the surface due to protonation under the preparation conditions [26].

VSM analysis: As illustrated in Fig. 1c, the VSM curve of MHA 3:1, 2.5:1, 2:1, 1.5:1, respectively magnetization at 20.44, 17.04, 15.51, and 13.82 emu/g. The magnetization (Ms) of MHA is strong to separation from MB by a magnet [40].

SEM-EDS analysis: Fig. 2 shows the SEM Image of HA and MHA 3:1, 2.5:1, 2:1, 1.5:1, respectively. HA and MHA have an irregular structure, the morphology of MHA is smoother than HA. The surface of MHA is smooth because it is prepared by hydrothermal process.

Analysis in Table 1 shows the Fe, C, and O atom percentages in HA and MHA. Fe atom appear after HA is composited into MHA. The percent mass of Fe atom in MHA were 3:1, 2.5:1, 2:1, 1.5:1, at 34.5 %, 31.5 %, 27.7 %, and 24.4 %, respectively. The percent mass of Fe atom decreases in line with the VSM analysis which decreases the magnetization. The percent mass of C atom decreased while the O atom increased, Fe-O bonds affect this to happen. Fe-O bonds in MHA were supported by FTIR analysis, a new peak appeared at 794 cm^{-1}. Therefore, the preparation of MHA has been a success.

Functional group of HA and MHA

The total acidity and carboxyl group of MHA 3:1, 2.5:1, 2:1, 1.5:1 was a drastic decrease from HA. The total acidity of MHA 3:1, 2.5:1, 2:1, 1.5:1 was decreased from 670 cmol/kg to 287.5, 317.50, 405, and 430 cmol/kg, respectively. The carboxyl group of MHA 3:1, 2.5:1, 2:1, 1.5:1 was decreased from 296 cmol/kg to 37.5, 59.33, 42, 44.67 cmol/kg, respectively. It is due to the preparation of MHA carried out under alkaline conditions (addition of NH_3). The carboxyl and phenolic hydroxyl groups are iodized and interact with Fe^{2+} and Fe^{3+} from Fe_3O_4 [49]. However, the carboxyl group is interacts more with Fe_3O_4 than the phenolic hydroxyl group, so the carboxyl group's reduction is very drastic. The total acidity, carboxyl group, and phenolic hydroxyl group as reported in Table 2.

Effect of point of zero charge pH (pHpzc)

pH is an important factor during the adsorption process. One of the appropriate methods is the point of zero charge, pHpzc [51]. Therefore, the effect of pH was investigated with pHpzc whose results are in Fig. 3. The meeting point between the initial and final pH shows no movement of H^+ ions, which means that this meeting point is that pHpzc, HA and MHA are in neutral conditions. According to Fig. 3, pHpzc of HA and MHA 3:1, 2.5:1, 2:1, 1.5:1 at 8.06, 5.82, 6.08, 4.80, and 4.76, respectively. HA and MHA are positively charged at pH lower than pHpzc and negatively charged at pH higher than pHpzc.

Adsorption kinetics

Adsorption kinetics describes the transfer of substances in the adsorption process and the factors that affect the adsorption rate [52]. PFO and PSO kinetic models were used to study the adsorption behavior of MB in HA and MHA. The adsorption kinetics of HA and MHA 3:1, 2.5:1, 2:1, 1.5:1 shown in Table 3. The five adsorbents were better at PSO in adsorption of MB, as evidenced by the correlation coefficient (R^2) PSO > PFO. PSO means that the adsorption process is chemisorption [53]. Chemisorption means that increase in the initial concentration of MB will also increase the adsorbed concentration, as shown in Fig. 4.

Adsorption isotherms

The adsorption isotherms describe the relationship between the adsorbent surface and the amount of adsorbate in the solution [54]. The Langmuir and Freundlich isotherm model were used to study the adsorption behavior of MB in HA and MHA. Adsorption isotherms of HA and MHA 3:1, 2.5:1, 2:1, 1.5:1 shown in Table 4. The adsorbents were better in the Langmuir model, as evidenced by the correlation coefficient (R^2) Langmuir > Freundlich. This shows the characteristics adsorption of MB by HA and MHA homogeneous (monolayer) and an increase in the initial concentration of MB will also increase the adsorbed concentration [55], as in Fig. 5. Maximum adsorption capacity of HA and MHA 3:1,

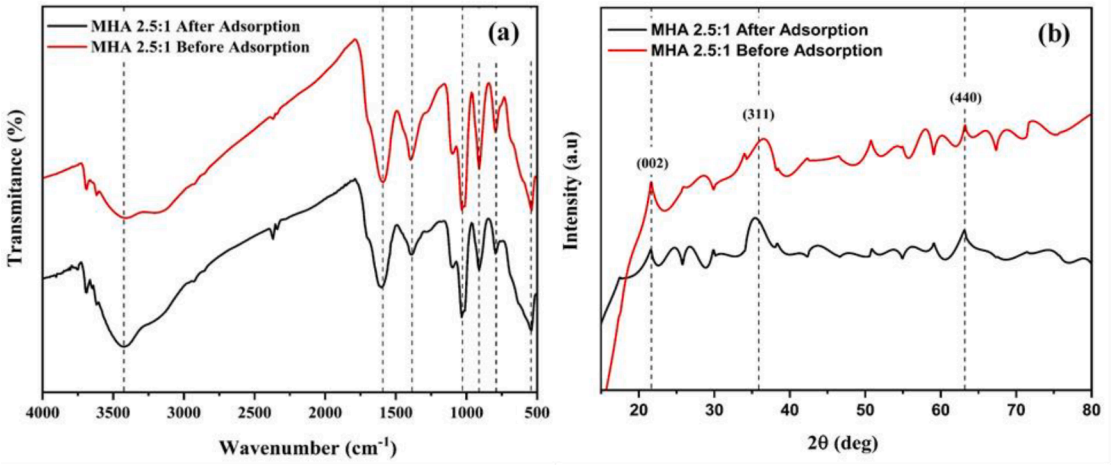

Fig. 7. FTIR spectra (a) and XRD patterns (b) of MHA 2.5:1 before and after adsorption.

2.5:1, 2:1, 1.5:1 at 66.225, 102.041, 161.290, 156.250, 138.889 mg/g, respectively. The highest maximum adsorption capacity is MHA 2.5:1. This adsorbent will be continued with regeneration. The comparison adsorption capacity of HA and MHA in adsorption of MB with other adsorbents is displayed in Table 5.

Adsorption thermodynamics

Adsorption thermodynamics describes the spontaneity and heat changes adsorption of MB by HA and MHA [61]. Adsorption thermodynamics are calculated and contained in Table 6. A negative Δ G value describes the spontaneity adsorption of MB by HA and MHA [62–63]. Δ G higher at the greater temperature. This proves that adsorption of MB by HA and MHA is more efficient at high temperatures. A positive value of Δ H indicates the endothermic adsorption of MB by HA and MHA. A positive value of Δ S indicates randomness at the solid–liquid interface during the adsorption process [64–65].

Regeneration of MHA

MHA 2.5:1 as adsorbent with the highest maximum adsorption capacity was followed by the regeneration process. Regeneration is very important for industry because adsorbents can be reused [66]. Moreover, MHA is easily separated with methylene blue solution using a magnet [67]. Fig. 6 shows regeneration of MHA 2.5:1 in MB adsorption–desorption cycles. MHA regeneration efficiency decreased from 92.28 % to 58.92 % in the fifth cycle. These results indicate the good recyclability of MHA to remove MB. The good recyclability of MHA indicates that MHA has good stability supported by FTIR spectra and XRD patterns after adsorption which shows no significant changes as in Fig. 7. The diffraction peaks at $2\theta = 20.40^\circ$ (002), 35.63° (311), and 63.3° (440) can still be observed. The peak at 3425 cm^{-1}, 1604 cm^{-1}, 1396, 1095 cm^{-1}, 1026 cm^{-1}, 910 cm^{-1}, 794 cm^{-1} and 540 cm^{-1} can still be observed..

Conclusion

Preparation of Magnetite Humic Acid (MHA) 3:1, 2.5:1, 2:1, and 1.5:1 was successful as evidenced by the characterization using FTIR, XRD, VSM, and SEM-EDS Analysis. The functional groups of MHA are total acidity, carboxyl group, and phenolic hydroxyl group. The carboxyl, and phenolic hydroxyl groups are iodized and interact with Fe^{2+} and Fe^{3+} from Fe_3O_4. However, the carboxyl group is interacts more with Fe_3O_4 than the phenolic hydroxyl group, so the carboxyl group's reduction is very drastic. pHpzc of HA and MHA 3:1, 2.5:1, 2:1, 1.5:1 at 8.06, 5.82, 6.08, 4.80, and 4.76, respectively. HA and MHA were better at PSO and Langmuir model in adsorption of MB. Maximum adsorption capacity of HA and MHA 3:1, 2.5:1, 2:1, 1.5:1 at 66.225, 102.041, 161.290, 156.250, 138.889 mg/g, respectively. The highest maximum adsorption capacity is MHA 2.5:1 (161.290 mg/g). MHA 2.5:1 will be continued with regeneration. MHA regeneration efficiency decreased from 92.28 % to 58.92 % in the fifth cycle. These results indicate the good recyclability and of MHA to remove MB supported by FTIR and XRD analysis after adsorption which shows no significant changes.

CRediT authorship contribution statement

Nur Ahmad: Conceptualization, Investigation, Writing – original draft, Software. **Fitri Suryani Arsyad:** Methodology, Validation, Visualization. **Idha Royani:** Visualization, Data curation, Formal analysis. **Aldes Lesbani:** Methodology , Conceptualization, Writing – review & editing, Supervision.

Declaration of Competing Interest

The authors declare that they have no known competing financial interests or personal relationships that could have appeared to influence the work reported in this paper.

Data availability

No data was used for the research described in the article.

Acknowledgement

Authors thank Research Center of Inorganic Materials and Complexes, Faculty of Mathematics and Natural Sciences, Sriwijaya University for instrumental analysis.

References

[1] S.S. Vedula, G.D. Yadav, Wastewater treatment containing methylene blue dye as pollutant using adsorption by chitosan lignin membrane: Development of membrane, characterization and kinetics of adsorption, Journal of the Indian Chemical Society 99 (1) (2022), 100263, https://doi.org/10.1016/j.jics.2021.100263.

[2] L.R. Bonetto, J.S. Crespo, R. Guégan, V.I. Esteves, M. Giovanela, Removal of methylene blue from aqueous solutions using a solid residue of the apple juice industry: Full factorial design, equilibrium, thermodynamics and kinetics aspects, J Mol Struct 1224 (2021), 129296, https://doi.org/10.1016/j.molstruc.2020.129296.

[3] M. Mariana, E.M. Mistar, T. Alfatah, M.D. Supardan, High-porous activated carbon derived from Myristica fragrans shell using one-step KOH activation for methylene blue adsorption, Bioresour Technol Rep vol. 16, no. August (2021), 100845, https://doi.org/10.1016/j.biteb.2021.100845.

[4] K. Karami, S.M. Beram, P. Bayat, F. Siadatnasab, A. Ramezanpour, A novel nanohybrid based on metal–organic framework MIL101−Cr/PANI/Ag for the adsorption of cationic methylene blue dye from aqueous solution, J Mol Struct 1247 (2022), 131352, https://doi.org/10.1016/j.molstruc.2021.131352.

[5] A. Lesbani, N.R. Palapa, R.J. Sayeri, T. Taher, N. Hidayati, High reusability of NiAl LDH/biochar composite in the removal methylene blue from aqueous solution, Indonesian Journal of Chemistry 21 (2) (2021) 421–434, https://doi.org/10.22146/ijc.56955.

[6] M. Sari Yilmaz Graphene oxide/hollow mesoporous silica composite for selective adsorption of methylene blue Microporous and Mesoporous Materials 330 November 2022 2021, p. 111570 10.1016/j.micromeso.2021.111570.

[7] Y. Zhang, H. Tan, C. Wang, B. Li, H. Yang, H. Hou, C. Xiao, TiO2-coated glass hollow fiber membranes: preparation and application for photocatalytic methylene blue removal, J Eur Ceram Soc 42 (5) (2022) 2496–2504.

[8] R. Muttaqin, R. Pratiwi, Ratnawati, E.L. Dewi, M. Ibadurrohman, Slamet, Degradation of methylene blue-ciprofloxacin and hydrogen production simultaneously using combination of electrocoagulation and photocatalytic process with Fe-TiNTAs, International Journal of Hydrogen Energy 47 (42) (2022) 18272–18284.

[9] K. Wu, M. Shi, X. Pan, J. Zhang, X. Zhang, T. Shen, Y. Tian, Decolourization and biodegradation of methylene blue dye by a ligninolytic enzyme-producing Bacillus thuringiensis: Degradation products and pathway, Enzyme Microb Technol 156 (2022) 109999.

[10] Z. Hu, C. Guo, P. Wang, R. Guo, X. Liu, Y.e. Tian, Electrochemical degradation of methylene blue by Pb modified porous SnO2 anode, Chemosphere 305 (2022) 135447.

[11] M.N. Sakib, N. Hano, M. Takafuji, S. Ahmed, Preparation of chitosan/laterite/iron oxide-based biocomposite and its application as a potential adsorbent for the removal of methylene blue from aqueous solution, Environ Nanotechnol Monit Manag 17 (2022) 100658.

[12] A. Ulu M. Alpaslan A. Gultek B. Ates Eco-friendly chitosan/κ-carrageenan membranes reinforced with activated bentonite for adsorption of methylene blue Mater Chem Phys 278 April 2021 2021, p. 125611 10.1016/j.matchemphys.2021.125611.

[13] Y. Mu, H. Ma, NaOH-modified mesoporous biochar derived from tea residue for methylene Blue and Orange II removal, Chemical Engineering Research and Design 167 (2021) 129–140, https://doi.org/10.1016/j.cherd.2021.01.008.

[14] S.A. Gupta, Y. Vishesh, N. Sarvshrestha, A.S. Bhardwaj, P.A. Kumar, N.S. Topare, S. Raut-Jadhav, S.A. Bokil, A. Khan, Adsorption isotherm studies of Methylene blue using activated carbon of waste fruit peel as an adsorbent, Mater Today Proc 57 (2022) 1500–1508.

[15] N. Normah, N. Juleanti, P.M.S.B.N. Siregar, A. Wijaya, N.R. Palapa, T. Taher, A. Lesbani, Size selectivity of anionic and cationic dyes using LDH modified adsorbent with low-cost rambutan peel to hydrochar, Bulletin of Chemical Reaction Engineering & Catalysis 16 (4) (2021) 869–880.

[16] S.K. Sriramoju, P.S. Dash, S. Majumdar, Meso-porous activated carbon from lignite waste and its application in methylene Blue adsorption and coke plant effluent treatment, J Environ Chem Eng 9 (1) (2021), 104784, https://doi.org/10.1016/j.jece.2020.104784.

[17] H. Niu, H. Yang, L. Tong, Adsorption behaviors of Au(III) onto humic acid extracted from gold ore: Adsorptive kinetics, isotherm and mechanism, Colloids Surf A Physicochem Eng Asp vol. 630, no. July (2021), 127442, https://doi.org/10.1016/j.colsurfa.2021.127442.
[18] Y. Shao M. Bao W. Huo R. Ye Y. Liu W. Lu Production of artificial humic acid from biomass residues by a non-catalytic hydrothermal process J Clean Prod 335 November 2022 2021, p. 130302 10.1016/j.jclepro.2021.130302.
[19] A.M. Tadini, A.C.C. Bernardi, D.M.B.P. Milori, P.P.A. Oliveira, J.R.M. Pezzopane, L. Martin-Neto, Spectroscopic characteristics of humic acids extracted from soils under different integrated agricultural production systems in tropical regions, Geoderma Regional 28 (June) (2021) 2022, https://doi.org/10.1016/j.geodrs.2021.e00476.
[20] E. Pramono, M.A. Zakaria, K.F. Fridiasari, S.T.C.L. Ndruru, M. Bagaskara, R. E. Mustofa, G.P.W. Sejati, C. Purnawan, O.A. Saputra, Cellulose derived from oil palm empty fruit bunches as filler on polyvinylidene fluoride based membrane for water containing humic acid treatment, Groundw Sustain Dev 17 (2022) 100744.
[21] A. Akaichi, A. Jebali, O. Abbes, S.H. Taieb, M. Feki, K. Kaboudi, R.B. Chaouacha-Chekir, M. Benlarbi, N. Boudhrioua, Effect of humic acid and organic acids, alone or in combination, on blood biochemical constituents and humoral immune response in broiler chickens, Livest Sci 258 (2022) 104880.
[22] Z.H. Sharafabad, M. Abdipour, M. Hosseinifarahi, A. Kelidari, L. Rashidi, "Integrated humic acid and vermicomposting changes essential oil quantity, and quality in field-grown Lavandula angustifolia L. intercropped with Brassica nigra L.", *Ind Crops*, Prod vol. 178, no. January (2022), 114635, https://doi.org/10.1016/j.indcrop.2022.114635.
[23] K. Wan, Y. Xiao, J. Fan, Z. Miao, G. Wang, S. Xue, Preparation of high-capacity macroporous adsorbent using lignite-derived humic acid and its multifunctional binding chemistry for heavy metals in wastewater, J Clean Prod 363 (2022) 132498.
[24] M. Lu, Y. Zhang, Y. Zhou, Z. Su, B. Liu, G. Li, T. Jiang, Adsorption-desorption characteristics and mechanisms of Pb(II) on natural vanadium, titanium-bearing magnetite-humic acid magnetic adsorbent, Powder Technol 344 (2019) 947–958.
[25] C. Li, S. Zhao, X. Huang, D. Xie, X. Li, J. Ma, Y. Liao, Development of humic acid based adsorbents for fast and efficient removal of ammonia and organic nitrogen from super magnetic separation treated wastewater, Journal of Environmental Chemical Engineering 10 (2) (2022) 107223.
[26] J. El Gaayda, F. Ezzahra Titchou, R. Oukhrib, I. Karmal, H. Abou Oualid, A. Berisha, H. Zazou, C. Swanson, M. Hamdani, R. Ait Akbour, Removal of cationic dye from coloured water by adsorption onto hematite-humic acid composite: Experimental and theoretical studies, Sep Purif Technol 288 (2022) 120607.
[27] Y. Zhang, M. Yin, X. Sun, J. Zhao, Implication for adsorption and degradation of dyes by humic acid: Light driven of environmentally persistent free radicals to activate reactive oxygen species, Bioresour Technol 307 (2020) 123183.
[28] P. Zhao, Z. Huang, Q. Ma, B. Zhang, P. Wang, Artificial humic acid synthesized from food wastes: An efficient and recyclable adsorbent of Pb (II) and Cd (II) from aqueous solution, Environ Technol Innov 27 (2022), 102399, https://doi.org/10.1016/j.eti.2022.102399.
[29] S. Lu, W. Liu, Y. Wang, Y. Zhang, P. Li, D. Jiang, C. Fang, Y. Li, An adsorbent based on humic acid and carboxymethyl cellulose for efficient dye removal from aqueous solution, Int J Biol Macromol 135 (2019) 790–797.
[30] E.L.M. Amutenya, F. Zhou, J. Liu, W. Long, L. Ma, M. Liu, G. Lv, Preparation of humic acid-bentonite polymer composite: A heavy metal ion adsorbent, Heliyon 8 (6) (2022) e09720.
[31] M. Maia, P. Barrulas, P. Nogueira, J. Mirão, F. Noronha, In situ LA-ICP-MS trace element analysis of magnetite as a vector towards mineral exploration: A comparative case study of Fe-skarn deposits from SW Iberia (Ossa-Morena Zone), J Geochem Explor 234 (July) (2021) 2022, https://doi.org/10.1016/j.gexplo.2021.106941.
[32] M.J. Al-Kheetan, T. Azim, J. Byzyka, S.H. Ghaffar, M.M. Rahman, Performance of magnetite-based stone mastic asphalt (SMA) as a superior surface course material, Constr Build Mater vol. 322, no. January (2022), 126463, https://doi.org/10.1016/j.conbuildmat.2022.126463.
[33] S. Jung, M. Kim, J. Lee, J. Shin, S.G. Shin, J. Lee, Effect of magnetite supplementation on mesophilic anaerobic digestion of phenol and benzoate: Methane production rate and microbial communities, Bioresour Technol vol. 350, no. March (2022), 126943, https://doi.org/10.1016/j.biortech.2022.126943.
[34] Y.M. Alexandrovskaya, Y.R. Pavley, Y.V. Grigoriev, V.V. Grebenev, T.B. Shatalova, M.V. Obrezkova, Thermal behavior of magnetite nanoparticles with various coatings in the range 30–1000 °C, Thermochimica Acta 708 (2022) 179120.
[35] A. Kalidason, T. Kuroiwa, Synthesis of chitosan–magnetite gel microparticles with improved stability and magnetic properties: A study on their adsorption, recoverability, and reusability in the removal of monovalent and multivalent azo dyes, React Funct Polym vol. 173, no. January (2022), 105220, https://doi.org/10.1016/j.reactfunctpolym.2022.105220.
[36] L. Zhang, F. Fu, G. Yu, G. Sun, B. Tang, Fate of Cr(VI) during aging of ferrihydrite-humic acid co-precipitates: Comparative studies of structurally incorporated Al(III) and Mn(II), Science of the Total Environment 807 (2022), 151073, https://doi.org/10.1016/j.scitotenv.2021.151073.
[37] M. Rashid, N.T. Price, M.Á. Gracia Pinilla, K.E. O'Shea, Effective removal of phosphate from aqueous solution using humic acid coated magnetite nanoparticles, Water Res 123 (3) (2017) 353–360, https://doi.org/10.1016/j.watres.2017.06.085.
[38] A. Esmaeilian, K.E. O'Shea, Application of dimensional analysis in sorption modeling of the styryl pyridinium cationic dyes on reusable iron based humic acid coated magnetic nanoparticles, Chemosphere 286 (2022) 131699.
[39] N. Ahmad, F. Suryani Arsyad, I. Royani, A. Lesbani, Selectivity of Malachite Green on Cationic Dye Mixtures Toward Adsorption on Magnetite Humic Acid, Environ Nat Resour J 20 (6) (2022) 1–10.
[40] S.J. Santosa, P.A. Krisbiantoro, M. Yuniarti, Kustomo, S. Koesnarpardi, Magnetically separable humic acid-functionalized magnetite for reductive adsorption of tetrachloroaurate(III) ion in aqueous solution, Environmental Nanotechnology, Monitoring & Management 15 (2021) 100454.
[41] P. Karthikeyan, S.S.D. Elanchezhiyan, H.A.T. Banu, M. Hasmath Farzana, C. M. Park, Hydrothermal synthesis of hydroxyapatite-reduced graphene oxide (1D–2D) hybrids with enhanced selective adsorption properties for methyl orange and hexavalent chromium from aqueous solutions, Chemosphere 276 (2021), 130200, https://doi.org/10.1016/j.chemosphere.2021.130200.
[42] J. Miao, X. Zhao, Y.X. Zhang, Z.L. Lei, Z.H. Liu, Preparation of hollow hierarchical porous CoMgAl-borate LDH ball-flower and its calcinated product with extraordinary adsorption capacity for Congo red and methyl orange, Appl Clay Sci vol. 207, no. April (2021), 106093, https://doi.org/10.1016/j.clay.2021.106093.
[43] X.i. Liu, Y. Wu, H. Ye, J. Chen, W. Xiao, W. Zhou, Z.N. Garba, I. Lawan, L. Wang, Z. Yuan, Modification of sugar-based carbon using lanthanum and cobalt bimetal species for effective adsorption of methyl orange, Environ Technol Innov 23 (2021) 101769.
[44] M. Muslim, A. Ali, I. Neogi, N. Dege, M. Shahid, M. Ahmad, Facile synthesis, topological study, and adsorption properties of a novel Co (II)-based coordination polymer for adsorptive removal of methylene blue and methyl orange dyes, Polyhedron vol. 210, no. July (2021), 115519, https://doi.org/10.1016/j.poly.2021.115519.
[45] S. Hussain, M. Kamran, S.A. Khan, K. Shaheen, Z. Shah, H. Suo, Q. Khan, A.B. Shah, W.U. Rehman, Y.O. Al-Ghamdi, U. Ghani, Adsorption, kinetics and thermodynamics studies of methyl orange dye sequestration through chitosan composites films, Int J Biol Macromol 168 (2021) 383–394.
[46] X. Sun, Y. Zhou, X. Zheng, Comparison of adsorption behaviors of Fe-La oxides co-loaded MgO nanosheets for the removal of methyl orange and phosphate in single and binary systems, J Environ Chem Eng 8 (5) (2020), 104252, https://doi.org/10.1016/j.jece.2020.104252.
[47] S.-Y. Wang, D. Xin, Z.-H. Zhou, Iron(II/III) sulfite and sulfates for oxygen adsorption and degradation of methyl orange, Journal of Solid State Chemistry 306 (2022) 122784.
[48] C.S. Stoicescu, D. Culita, N. Stanica, F. Papa, R.N. State, G. Munteanu, Temperature programmed reduction of a core-shell synthetic magnetite: Dependence on the heating rate of the reduction mechanism, Thermochim Acta vol. 709, no. January (2022), 179146, https://doi.org/10.1016/j.tca.2022.179146.
[49] S. Koesnarpadi, S.J. Santosa, D. Siswanta, B. Rusdiarso, Synthesis and Characterizatation of Magnetite Nanoparticle Coated Humic Acid (Fe3O4/HA), Procedia Environ Sci 30 (Jan. 2015) 103–108, https://doi.org/10.1016/J.PROENV.2015.10.018.
[50] F.J. Stevenson, Humus chemistry: genesis, composition, reactions, John Wiley & Sons, 1994.
[51] W. Zhang, T. Huang, Y.u. Ren, Y. Wang, R. Yu, J. Wang, Q. Tu, Preparation of chitosan crosslinked with metal-organic framework (MOF-199)@aminated graphene oxide aerogel for the adsorption of formaldehyde gas and methyl orange, Int J Biol Macromol 193 (2021) 2243–2251.
[52] X. Liu, Y. Guo, C. Zhang, X. Huang, K. Ma, Y. Zhang, Preparation of graphene oxide/4A molecular sieve composite and evaluation of adsorption performance for Rhodamine B, Separation and Purification Technology 286 (2022) 120400.
[53] X. Chen, H. Li, W. Liu, X. Zhang, Z. Wu, S. Bi, W. Zhang, H. Zhan, Effective removal of methyl orange and rhodamine B from aqueous solution using furfural industrial processing waste: Furfural residue as an eco-friendly biosorbent, Colloids Surf A Physicochem Eng Asp 583 (2019) 123976.
[54] K. Shen, M.A. Gondal, Removal of hazardous Rhodamine dye from water by adsorption onto exhausted coffee ground, Journal of Saudi Chemical Society 21 (2017) S120–S127, https://doi.org/10.1016/j.jscs.2013.11.005.
[55] T.J.M. Fraga, L.E.M. de Lima, Z.S.B. de Souza, M.N. Carvalho, E.M.P.d.L. Freire, M. G. Ghislandi, M.A. da Motta, Amino-Fe3O4-functionalized graphene oxide as a novel adsorbent of Methylene Blue: kinetics, equilibrium, and recyclability aspects, Environmental Science and Pollution Research 26 (28) (2019) 28593–28602.
[56] P. Su, Q. Wan, Y. Yang, J. Shu, H. Zhao, W. Meng, B. Li, M. Chen, Z. Liu, R. Liu, Hydroxylation of electrolytic manganese anode slime with EDTA-2Na and its adsorption of methylene blue, Separation and Purification Technology 278 (2021) 119526.
[57] S.D.K. Seera, D. Kundu, P. Gami, P.K. Naik, T. Banerjee, Synthesis and characterization of xylan-gelatin cross-linked reusable hydrogel for the adsorption of methylene blue, Carbohydrate Polymers 256 (2021) 117520.
[58] M.M. Motawea, M.A.T. Hussein, M.M. Elsenety, H.M. Ali, T.A. Seaf El-Nasr, H. Gomaa, Mesoporous hierarchical ZrO2@rice straw-derived SiO2 nanocomposite for rapid adsorption and sunlight-driven photocatalytic degradation of methylene blue, Journal of Photochemistry and Photobiology A: Chemistry 426 (2022) 113758.
[59] N. Zida Rosly, S. Ishak, A. Halim Abdullah, M. Ahmad Kamarudin, S. Efliza Ashari, S. Ainliah Alang Ahmad,, Fabrication and Optimization Calix[8]arene-PbS Nanoadsorbents for the Adsorption of Methylene Blue: Isotherms, Kinetics and Thermodynamics Studies, Journal of Saudi Chemical Society 26 (1) (2021), 101402, https://doi.org/10.1016/j.jscs.2021.101402.
[60] C. Dixit, M.C. Ncibi, M.L. Bernard, B. Sanjuan, S. Gaspard, The valorization of raw and chemically-modified silica residues from Bouillante geothermal power plant (Guadeloupe, FWI) for the removal of methylene blue and lead from aqueous media, J Environ Chem Eng 8 (5) (2020), 104285, https://doi.org/10.1016/j.jece.2020.104285.

[61] R.J.M. Nascimento, K.R.A. Pereira, F. Avelino, Parametric and modeling studies of Rhodamine-B adsorption using coconut coir-based materials as eco-friendly adsorbents, J Environ Chem Eng 9 (5) (2021) pp, https://doi.org/10.1016/j.jece.2021.105943.

[62] N.R. Palapa, T. Taher, A. Wijaya, A. Lesbani, Modification of cu/cr layered double hydroxide by keggin type polyoxometalate as adsorbent of malachite green from aqueous solution, Science and Technology Indonesia 6 (3) (2021) 209–217, https://doi.org/10.26554/sti.2021.6.3.209-217.

[63] A. Wijaya, P.M.S.B.N. Siregar, A. Priambodo, N.R. Palapa, T. Taher, A. Lesbani, "Innovative Modified of Cu-Al/C (C = Biochar, Graphite) Composites for Removal of Procion Red from Aqueous Solution", *Science and Technology*, Indonesia 6 (4) (2021) pp, https://doi.org/10.26554/sti.2021.6.4.228-234.

[64] P.M.S.B.N. Siregar, N.R. Palapa, A. Wijaya, E.S. Fitri, A. Lesbani, Structural stability of ni/al layered double hydroxide supported on graphite and biochar toward adsorption of congo red, Science and Technology Indonesia 6 (2) (2021) 85–95, https://doi.org/10.26554/STI.2021.6.2.85-95.

[65] Y. Zhao, L. Zhu, W. Li, J. Liu, X. Liu, K. Huang, Insights into enhanced adsorptive removal of Rhodamine B by different chemically modified garlic peels: Comparison, kinetics, isotherms, thermodynamics and mechanism, J Mol Liq 293 (2019), 111516, https://doi.org/10.1016/j.molliq.2019.111516.

[66] Y. Zhang, H. Han, X. Wang, M. Zhang, Y. Chen, C. Zhai, H. Song, J. Deng, J. Sun, C. Zhang, Utilization of NaP zeolite synthesized with different silicon species and NaAlO2 from coal fly ash for the adsorption of Rhodamine B, Journal of Hazardous Materials 415 (2021) 125627.

[67] A.M.S. Baptisttella, C.M.B.d. Araujo, M.P. da Silva, G.F.O.d. Nascimento, G.R.B. d. Costa, B.F. do Nascimento, M.G. Ghislandi, M.A.d. Motta Sobrinho, Magnetic Fe3O4-graphene oxide nanocomposite–synthesis and practical application for the heterogeneous photo-Fenton degradation of different dyes in water, Separation Science and Technology (Philadelphia) 56 (2) (2021) 425–438.